Supplementary Figures and Tables

Simultaneous Phase and Electronic Structure Regulation of MoC via B,N-Doping and Bimetallic Synergy for Efficient Hydrogen Evolution

Tongzhou Hong[1,2,#], Fuxiang He[2,#], Jin Jia[2,*], Shaowei Zhang[1,2], Dandan Lu[2], Chenxin Li[2], Yuanyuan Zhu[2], Guang Zhu[1,2,*]

[1] School of Mechanics and Optoelectronics Physics, Anhui University of Science and Technology, Huainan 232001, China. E-mail: guangzhu@ahszu.edu.cn

[2] Key Laboratory of Spin Electron and Nanomaterials of Anhui Higher Education Institutes, Suzhou University, Suzhou 234000, China. E-mail: jiajin@ahszu.edu.cn

[#] Tongzhou Hong and Fuxiang He contributed equally to this work.

*Corresponding authors.

E-mail addresses: jiajin@ahszu.edu.cn (J. Jia); guangzhu@ahszu.edu.cn (G. Zhu)

1 Experimental Methods

1.1 Experimental Reagents

The Anderson-type polyoxometalate $(NH_4)_4[NiH_6Mo_6O_{24}]\cdot 5H_2O$ (denoted as $NiMo_6$) was synthesized following a previously reported method.[1] Nickel nitrate hexahydrate ($Ni(NO_3)_2\cdot 6H_2O$), ammonium molybdate tetrahydrate ($(NH_4)_6Mo_7O_{24}\cdot 4H_2O$), cobalt chloride hexahydrate ($CoCl_2\cdot 6H_2O$), 2-methylimidazole ($C_4H_6N_2$), magnesium diboride (MgB_2), and magnesium chloride ($MgCl_2$) were all of analytical grade and used as received without further purification. Deionized water (resistivity ≥8.2 MΩ·cm) was used throughout the experiments.

1.2 Synthesis of Co,Ni-MoC@BNC

First, 0.24 g of $NiMo_6$, 0.12 g of $CoCl_2\cdot 6H_2O$, and 0.082 g of $C_4H_6N_2$ were placed in a mortar and ground thoroughly for 15 min. Subsequently, 0.138 g of MgB_2 and 1.45 g of $MgCl_2$ were added, and the mixture was ground for an additional 20 minutes to obtain a homogeneous mixture. The powder was spread in a porcelain boat, wrapped in copper foil, and positioned in the center of a tube furnace. Under an H_2/Ar atmosphere (10:90 volume ratio), the temperature was ramped to 750 °C at a rate of 5 °C min^{-1} and maintained for 4 h. After cooling naturally to room temperature, the product was collected and sonicated in a 1 M HCl solution to remove impurities. It was then washed alternately with deionized water and ethanol several times and finally dried in a vacuum oven at 60 °C to obtain the target catalyst, denoted as Co,Ni-MoC@BNC.

1.3 Synthesis of Co,Ni-Mo_xC@NC

The synthesis procedure for Co,Ni-Mo_xC@NC was identical to that of Co,Ni-MoC@BNC, with the exception that MgB_2 was excluded. This sample was prepared to investigate the influence of boron doping on the structural and catalytic properties.

1.4 Synthesis of Ni-MoC@BNC

The synthesis of Ni-MoC@BNC followed the same protocol as Co,Ni-MoC@BNC without the addition of $CoCl_2\cdot 6H_2O$. This control sample was used to evaluate the specific role of Co species within the catalytic system.

1.5 Materials Characterizations

X-ray diffraction (XRD) patterns were recorded using a Rigaku SmartLab 3KW diffractometer. Raman spectra were acquired on a Horiba Jobin Yvon Xplora Plus spectrometer with an excitation wavelength of 532 nm. Specific surface area and pore structure were analyzed using a Micromeritics ASAP 2020 Plus HD88 automated gas adsorption analyzer based on N_2 adsorption-desorption isotherms. The surface area was calculated using the Brunauer-Emmett-Teller (BET) model, while the mesopore distribution was analyzed via the

Barrett-Joyner-Halenda (BJH) model. Microscopic morphology and crystal structure were characterized by scanning electron microscopy (SEM, Hitachi Regulus 8100, operated at 5.0 kV) and transmission electron microscopy (TEM, JEOL JEM-2100F, operated at 200 kV). Energy-dispersive X-ray spectroscopy (EDS) was performed using a second-generation OXFORD-Xplore detector attached to the TEM system. Surface elemental composition and chemical valence states were analyzed using X-ray photoelectron spectroscopy (XPS, Thermo Scientific K-Alpha).

1.6 Electrochemical Measurements

Electrochemical performance was evaluated using a CHI 760E electrochemical workstation (Shanghai Chenhua) in a standard three-electrode system with 0.5 M H_2SO_4 as the electrolyte. The working electrode was prepared as follows: 10 mg of the sample was dispersed in a solution containing 150 μL of ethanol and 850 μL of deionized water, followed by sonication for approximately 20 min to form a homogeneous ink. Subsequently, 3.5 μL of the catalyst dispersion was drop-cast onto a glassy carbon electrode (GCE, area: 0.07065 cm^2). After drying at room temperature, 2 μL of 0.5 wt% Nafion solution was applied and air-dried. The resulting catalyst loading was 0.495 mg cm^{-2}. A commercial 10% Pt/C electrode (purchased from Aladdin) was prepared using the same method for comparison. In the three-electrode configuration, a saturated calomel electrode (SCE, saturated KCl) and a graphite rod served as the reference and counter electrodes, respectively. Potentials were calibrated to the reversible hydrogen electrode (RHE) scale using the Nernst equation: $E_{RHE} = E_{SCE} + 0.253 + 0.059 \times pH$.

Specific electrochemical testing protocols were as follows: Linear sweep voltammetry (LSV) was conducted at a scan rate of 2 mV s^{-1} in the potential range of 0 to −0.547 V vs. RHE. Tafel slopes were derived from the corresponding LSV curves. Electrochemical impedance spectroscopy (EIS) was performed at a bias of −0.22 V vs. RHE over a frequency range of 100 kHz to 0.01 Hz with an AC amplitude of 5 mV. The electrochemical double-layer capacitance (C_{dl}) was determined via cyclic voltammetry (CV) at various scan rates (10–100 mV s^{-1}) within the non-faradaic region of 0.093–0.193 V vs. RHE. Stability was assessed by cycling the potential 2000 times between 0 and −0.3 V vs. SCE at 50 mV s^{-1} (cyclic stability), and by performing a long-term chronopotentiometric test at a constant current density of 15 mA cm^{-2} for 30 h. Unless otherwise specified, all tests were performed at room temperature without iR compensation.

1.7 Density Functional Theory Calculations

To gain insights into the electronic structure and reaction mechanisms, DFT calculations were performed using the Vienna Ab-initio Simulation Package (VASP).[2] The exchange-correlation functional was described by the Perdew-Burke-Ernzerhof (PBE) formulation within the Generalized Gradient Approximation (GGA).[3] The plane-wave cutoff energy was set to 520

eV to ensure basis set convergence. For structural optimization, the Brillouin zone was sampled using a 5×5×1 Monkhorst-Pack k-point grid, with convergence criteria for energy and force set to 10^{-6} eV and 0.01 eV $Å^{-1}$, respectively. Van der Waals interactions were corrected using the DFT-D3 method[4] with Becke-Johnson damping. Finally, electronic properties such as charge density difference and Projected Density of States (pDOS) were analyzed using VESTA and VASPKIT software. All calculation parameters were pre-tested to ensure reliability and reproducibility.

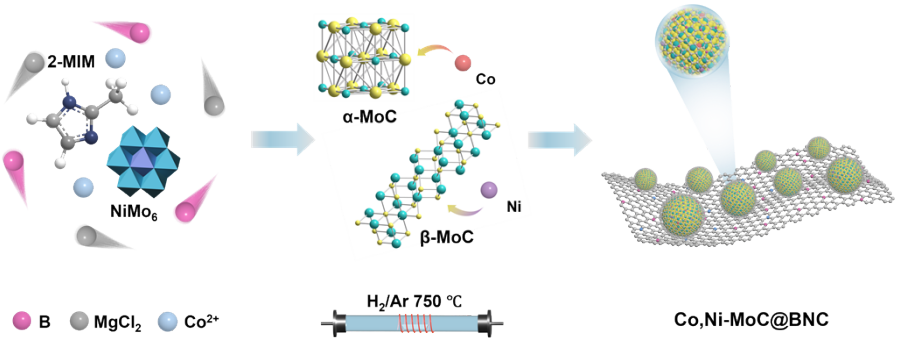

Fig. S1 Schematic illustration of the synthesis process for the Co,Ni-MoC@BNC electrocatalyst.

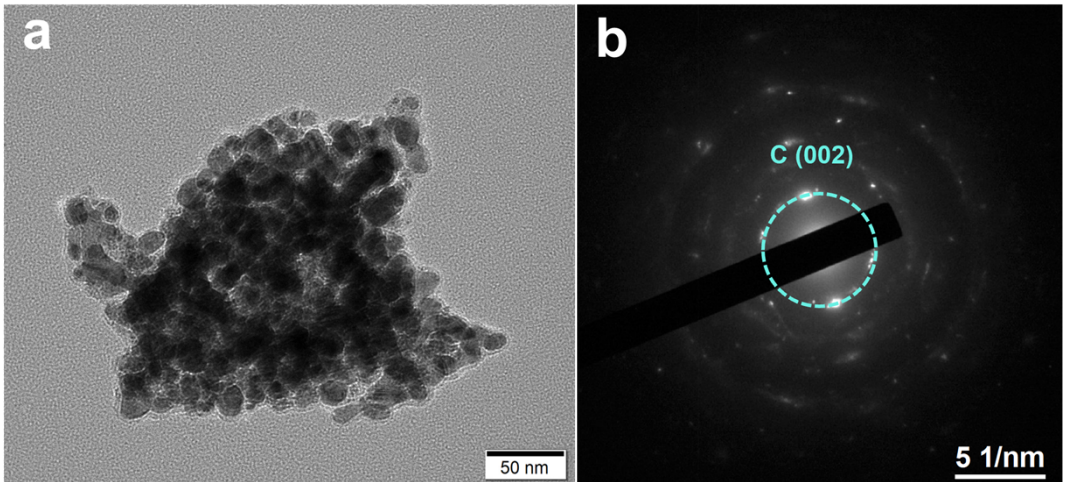

Fig. S2 (a) SEM image of Co,Ni-MoC@BNC. (b) The corresponding selected area electron diffraction (SAED) pattern.

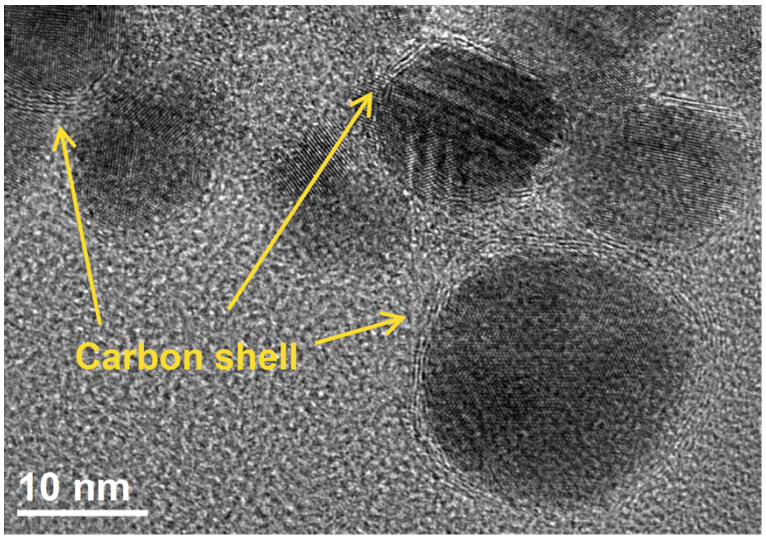

Fig. S3 Schematic illustration of the carbon layer in Co,Ni-MoC@BNC.

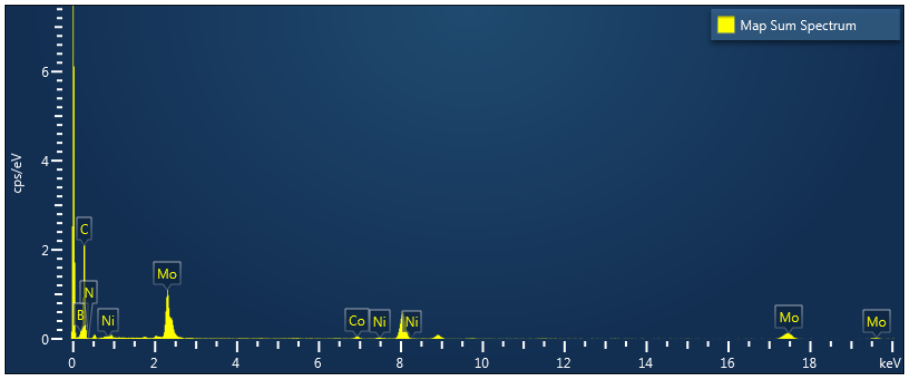

Fig. S4 The original cumulative EDS spectrum of the Co,Ni-MoC@BNC catalyst, showing the presence of Co, Ni, Mo, C, B, and N elements.

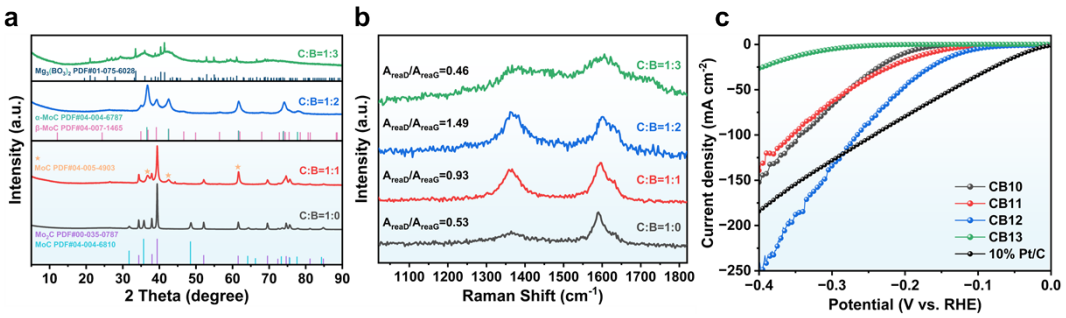

Fig. S5 (a) XRD patterns, (b) Raman spectra, and (c) LSV curves of samples synthesized with different B-doping levels.

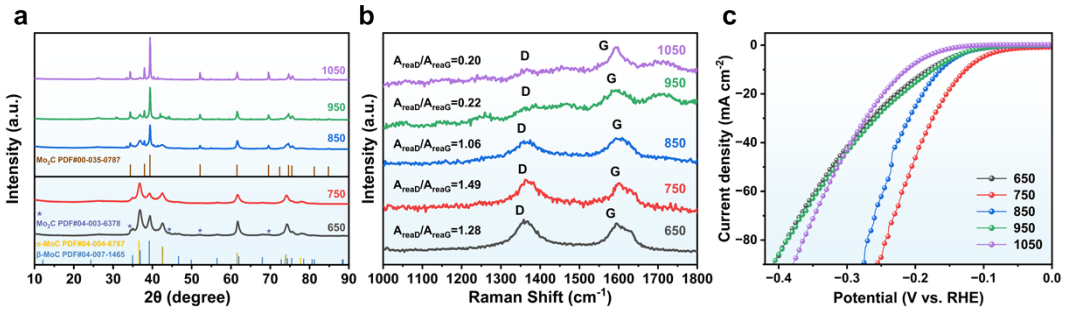

Fig. S6 (a) XRD patterns, (b) Raman spectra, and (c) LSV curves of samples prepared at different carbonization temperatures.

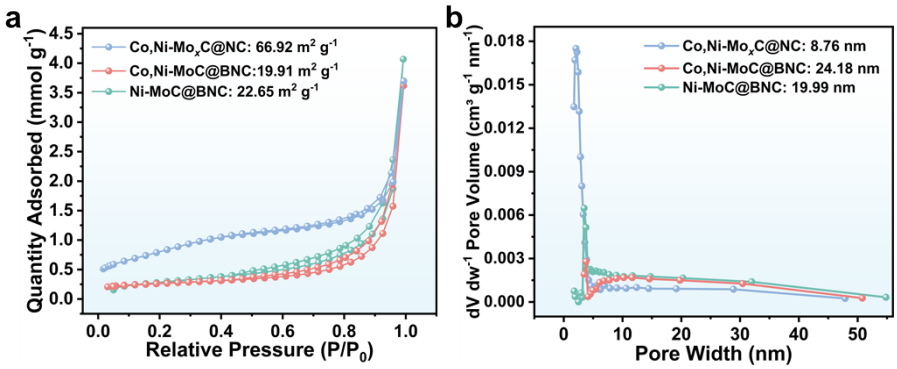

Fig. S7 (a) N_2 adsorption-desorption isotherms and (b) pore size distributions of Co,Ni-MoC@BNC, Co,Ni-Mo$_x$C@NC, and Ni-MoC@BNC.

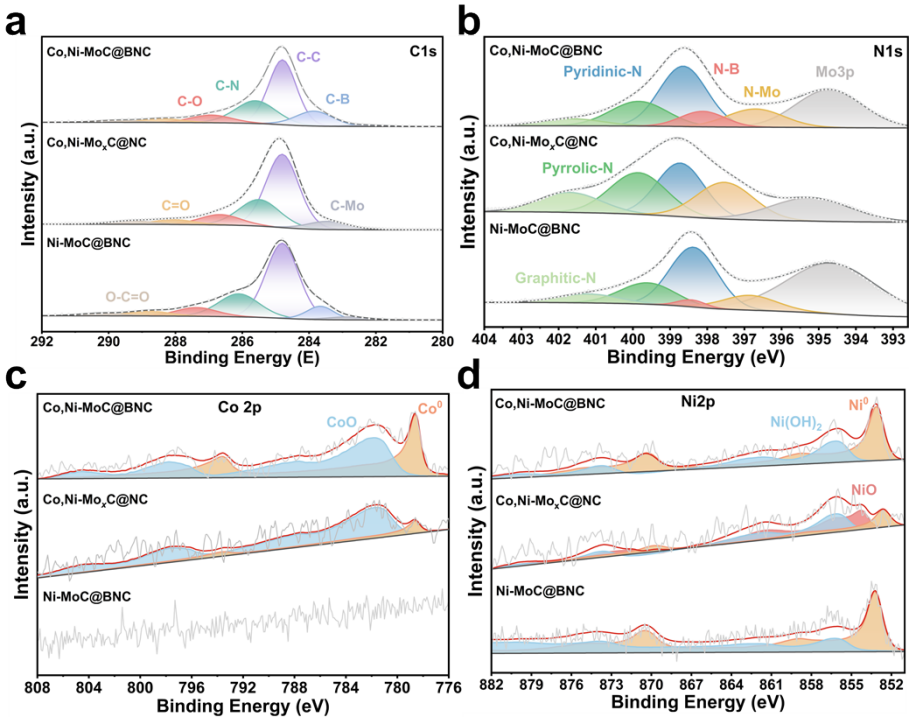

Fig. S8 XPS spectra of Co,Ni-MoC@BNC, Co,Ni-Mo$_x$C@NC, and Ni-MoC@BNC: (a) C 1s, (b) N 1s, (c) Co 2p, and (d) Ni 2p. The circles and gray lines represent the raw data, while the black and red lines represent the fitted data.

As shown in Fig. S8a, the binding energy at 284.8 eV corresponds to the sp^3 hybridized carbon of the functionalized graphene. The peaks located at 283.85, 285.6, 282.26, 286.92, 288.39, and 289.81 eV are assigned to C-B, C-N, Mo-C, C-O, C=O, and O-C=O bonds, respectively. The presence of C-B and C-N bonds confirms the successful incorporation of B and N atoms into the carbon framework (Fig. S8b). Notably, the Mo-C binding energy is located at a relatively low value of 282.26 eV; this is attributed to the electron donation from the B dopants, which increases the electron density of the C atoms within the Mo-C bonds, resulting in a negative shift in binding energy.

Crucially, the analyses of Co 2p (Fig. S8c) and Ni 2p (Fig. S8d) reveal the pivotal role of B-doping. The peak area of metallic Co^0 (778.6/793.6 eV) in Co,Ni-MoC@BNC is significantly larger than that in Co,Ni-Mo$_x$C@NC (781.8/797.4 eV). Similarly, the enhancement of the characteristic metallic Ni^0 peak demonstrates that B-doping significantly lowers the energy barrier during pyrolysis, facilitating the efficient reduction of Co/Ni species to their metallic states.[5, 6] These atomically dispersed metallic Co/Ni sites (Co^0/Ni^0), combined with the "Co/Ni-MoC" interfaces formed with the MoC lattice, constitute the key active centers responsible for the subsequent enhancement in electrocatalytic activity.

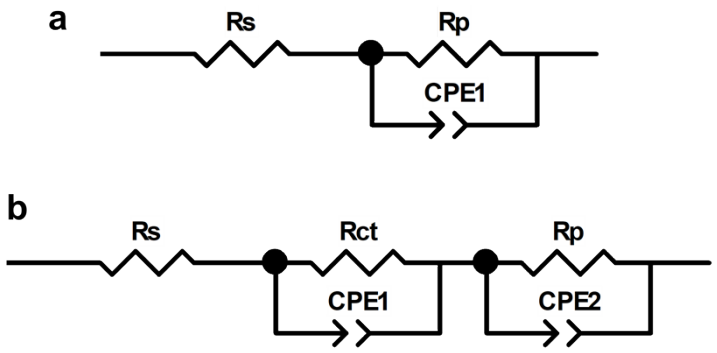

Fig. S9 Equivalent circuit models for (a) Ni-MoC@BNC and Pt/C, and (b) Co,Ni-MoC@BNC and Co,Ni-Mo_xC@NC.

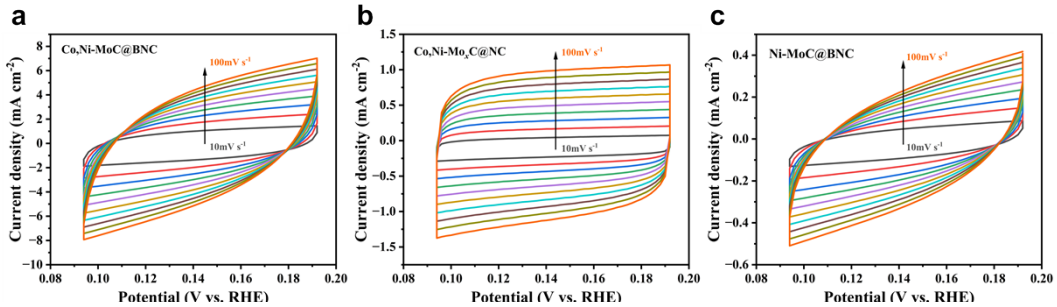

Fig. S10 Cyclic voltammetry (CV) curves of (a) Co,Ni-MoC@BNC, (b) Co,Ni-Mo_xC@NC, and (c) Ni-MoC@BNC.

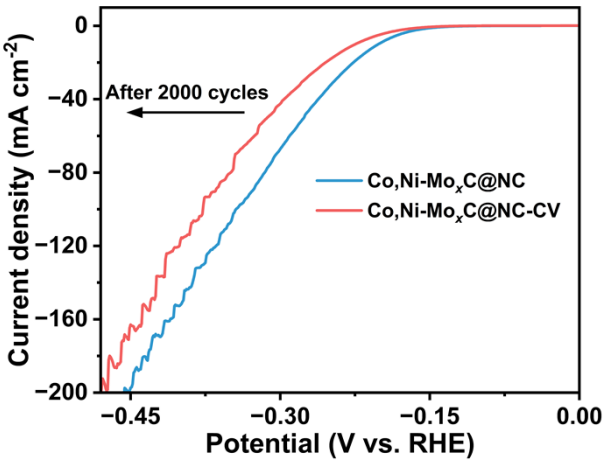

Fig. S11 Comparison of LSV curves of Co,Ni-Mo_xC@NC before and after 2000 CV cycles.

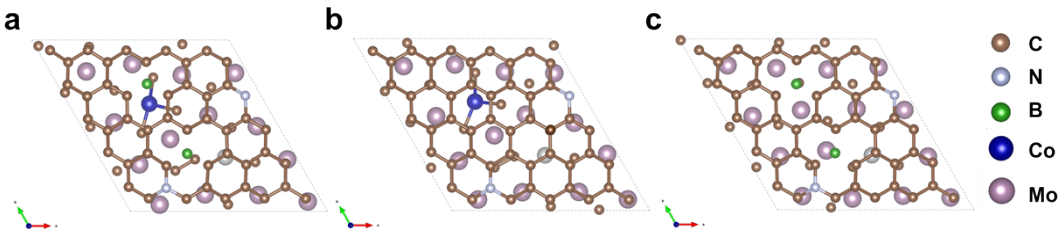

Fig. S12 Optimized crystal structure models of (a) Co,Ni-MoC@BNC, (b) Co,Ni-Mo_xC@NC, and (c) Ni-MoC@BNC.

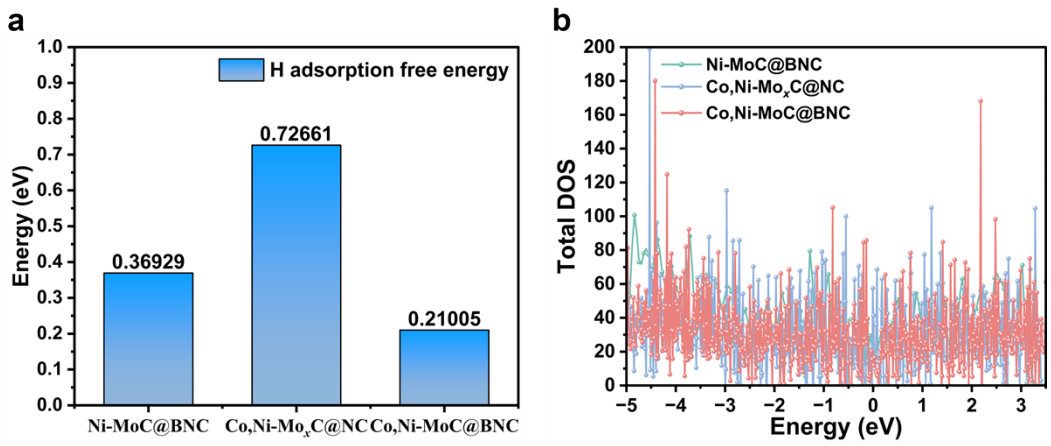

Fig. S13 (a) Calculated Gibbs free energy of hydrogen adsorption (ΔG_{H*}) and (b) Total Density of States (TDOS) plots for Co,Ni-MoC@BNC, Co,Ni-Mo$_x$C@NC, and Ni-MoC@BNC.

Table S1. Elemental analysis results of Co,Ni-MoC@BNC catalysts.

Element	Line Type	k Factor	k Factor type	Absorption Correction	Wt%	Wt% Sigma	Atomic %
B	K series	3.627	Theoretical	1	0	0	0
C	K series	1.341	Theoretical	1	53.56	0.78	89.96
N	K series	1.702	Theoretical	1	0	0	0
Co	K series	0.574	Theoretical	1	1.49	0.12	0.51
Ni	K series	0.563	Theoretical	1	0.59	0.1	0.2
Mo	L series	0.875	Theoretical	1	44.37	0.78	9.33
Total					100		100

Table S2. Bader charge analysis.

	Co,Ni-MoC@BNC	Ni-MoC@BNC	Co,Ni-Mo_xC@NC
Electron gain of H^* (e)	0.192	0.184	0.046

Table S3. Comparison of the HER performance of Co,Ni-MoC@BNC with other reported electrocatalysts.

Catalyst	Electrolyte	Overpotential η_{10}（mV）	Tafel slope (mV dec^{-1})	C_{DL} (mF cm^{-2})	Loading mass (mg/cm^2)	Ref
B-MoC	0.5 M H_2SO_4	285	128	17.28	~	7
Co-MoC/Mo_2C-0.5	0.5 M H_2SO_4	114	54	17.9	0.57	8
N-Mo_2C/PC	0.5 M H_2SO_4	109	37	47.9	1.12	9
mNC-MoC/Ti_3C_2	0.5 M H_2SO_4	159	70.9	18.11	0.2	10
Mo_2C@NC/Mo_2C	0.5 M H_2SO_4	150	60	69.8	0.32	11
Mo_2C/Mo_3N_2/C	0.5 M H_2SO_4	121	59.4	76.35	1.41	12
B, N-Mo_2C	0.5 M H_2SO_4	144	85.5	10.9	~	13
Mo_2C/MoO_2/C	0.5 M H_2SO_4	141	71.21	60.10	1.41	14
Mo_2C/N-C/CW	0.5 M H_2SO_4	130.9	71.83	11.4	~	15
Co,Ni-MoC@BNC	0.5 M H_2SO_4	127	80.8	38.7	0.49	**This work**

Ref. Supplementary References

1 Y. Huang, Y. Sun, X. Zheng, T. Aoki, B. Pattengale, J. Huang, X. He, W. Bian, S. Younan, N. Williams, J. Hu, J. Ge, N. Pu, X. Yan, X. Pan, L. Zhang, Y. Wei and J. Gu, *Nat. Commun.*, 2019, **10**, 982.

2 G. Kresse and J. Furthmüller, *Comput. Mater. Sci.*, 1996, **6**, 15-50.

3 M. Ernzerhof and G. E. Scuseria, *J. Chem. Phys.*, 1999, **110**, 5029-5036.

4 J. Moellmann and S. Grimme, *J. Phys. Chem. C*, 2014, **118**, 7615-7621.

5 J. Liu, Y. Guo, X.-Z. Fu, J.-L. Luo and C. Zhi, *Green Energy Environ.*, 2023, **8**, 459-469.

6 H. Lin, N. Liu, Z. Shi, Y. Guo, Y. Tang and Q. Gao, *Adv. Funct. Mater.*, 2016, **26**, 5590-5598.

7 Q. Lin, C. Shang, Z. Chen, X. Wang and G. Zhou, *Int. J. Hydrogen Energy*, 2020, **45**, 30659-30665.

8 J. Li, R. Ge, P. Lan, J. Yang, J. Feng, Y. Li, S. Li, B. Liu and W. Li, *J. Mater. Chem. A*, 2022, **10**, 10493-10502.

9 L. Zheng, C. Liu, S. Wang, B. Gao, X. Fan, S. Xu, Y. Jia, Y. Zhang, Q. Gao, X. Cao and Y. Tang, *Mater. Today Energy*, 2022, **26**, 100992.

10 Y. Tang, C. Yang, Y. Xie, Y. Kang, W. Que, J. Henzie and Y. Yamauchi, *ACS Sustainable Chem. Eng.*, 2023, **11**, 168-176.

11 X. Zhang, T. Lei, M. Xia, Q.-H. Wei and Z. Xie, *Dalton Trans.*, 2023, **52**, 6267-6272.

12 G. Tian, B. Yao, G. Han, Y. Li, K. Zhang and J. Meng, *J. Mater. Chem. A*, 2023, **11**, 6581-6590.

13 S. Wang, S. Zhu, Z. Cui, Z. Li, S. Wu, W. Xu, Z. Gao, Y. Liang and H. Jiang, *J. Mater. Chem. A*, 2025, **13**, 3084-3093.

14 G. Tian, W. Qu, K. Zhang, J. Wu, W. Huang, R. Gu, G. Han and W. Wang, *ACS Sustainable Chem. Eng.*, 2025, **13**, 10780-10793.

15 K. Wang, S. Jiang, R. Zeng, L. Zeng, Y. Ou, J. Lv, X. Su, B. Chi, T. Wang and D. Dang, *Int. J. Hydrogen Energy*, 2025, **169**, 150556.